ELSEVIER

Contents lists available at ScienceDirect

## Soil Dynamics and Earthquake Engineering

journal homepage: www.elsevier.com/locate/soildyn



# Centrifuge modeling-of-models investigation on earthquake-induced excess pore pressure behavior of silty sand



Mohamed E. Ghazy a,b, Tarek Abdoun c, Ricardo Dobry, Waleed El-Sekelly d,d,\*

- a New York University Abu Dhabi, Abu Dhabi, United Arab Emirates
- <sup>b</sup> Arab Academy for Science, Technology and Maritime Transport, Alexandria, Egypt
- <sup>c</sup> Rensselaer Polytechnic Institute, Troy, NY, 12180, USA
- d Department of Structural Engineering, Mansoura University, Mansoura, 35516, Egypt

#### ARTICLE INFO

Keywords: Centrifuge modeling Liquefaction Silty sand Modeling of models

#### ABSTRACT

Two centrifuge experiments conducted at Rensselaer Polytechnic Institute (RPI) aimed to evaluate the effectiveness of the used centrifuge scaling laws and validate results obtained within the project, related to the liquefaction behavior of silty sand soils under simulated field drainage conditions. These experiments, replicating a 5-m thick silty sand layer under 1 atm overburden pressure and featuring a double drainage condition, were performed at two different centrifugal accelerations. Due to the difficulties encountered in saturating silty sand, this paper presents a bottom-up saturation method, verified through assessments of remaining air volume after saturation. Despite differing g-levels, the tests consistently demonstrated similar behaviors in terms of acceleration, pore pressure buildup and dissipation, and stress-strain responses, validating the saturation and modeling technique for silty sand.

## 1. Introduction

Geotechnical centrifuge model testing has long been recognized as an indispensable tool for investigating and analyzing challenges in geotechnical engineering. Since the 1980s, the practice of conducting scaled-down tests of geotechnical systems under dynamic conditions has become a standard approach, providing valuable insights into intricate design problems [1]. The geotechnical centrifuge, recognized for its enduring effectiveness and precision, employs established scaling laws of similitude specifically tailored for centrifuge model testing [2]. These laws, particularly those addressing the simulation of phenomena such as coupled consolidation and dynamics, were further refined by Kutter [3].

Ensuring the accuracy of scaling laws is an essential component of geotechnical centrifuge experimentation. The technique known as "modeling of models", which conducts comparative analyses on identical prototypes across different scaling factors, has been established as a robust method for thorough validation, as evidenced by several researchers [1,4–6]. This approach has facilitated a wide array of investigations, from the study of laterally loaded pile behavior [7–9], to the examination of temperature migration within soils [10–13]. Additionally, it has been applied to diverse subjects such as the scaling of debris flows [14], and understanding the onset and development of

static liquefaction in submerged slopes [15]. The versatility of this method has also been demonstrated in studies of internal erosion [16] and the intricate dynamics of seismic soil-structure interaction, as explored by Alisawi et al. [17]. The widespread application of the "modeling of models" technique emphasizes the geotechnical centrifuge's role as a key instrument, showcasing its versatility. It also illuminates the critical validation processes necessary to guarantee the findings' dependability and relevance in geotechnical engineering studies and design evaluations.

In addition to conventional centrifuge scaling laws, innovative approaches such as the "two-stage" scaling method proposed by Iai et al. [18], also known as generalized scaling laws, have been introduced to address challenges in testing large prototypes that exceed conventional dimensions. Substantiating the application of generalized centrifuge scaling laws, Tobita et al. [19] demonstrated the efficacy of the modeling of models technique in dynamic centrifuge tests for pile foundations. Moreover, Korre et al. [20] and Tobita et al. [21] utilized this technique to validate the generalized scaling laws in the context of liquefiable sloping deposits within the Liquefaction Experiments and Analysis Projects (LEAP). Ma et al. [22] introduced a scaling law ensuring equivalent shear strain between the model and the prototype, addressing concerns related to scaling shear strain in the generalized

<sup>\*</sup> Corresponding author. New York University Abu Dhabi, Abu Dhabi, United Arab Emirates. *E-mail addresses*: we20@nyu.edu, welsekelly@mans.edu.eg (W. El-Sekelly).

centrifuge scaling laws proposed by Iai et al. [18].

This paper focuses on the application of the "modeling of models" technique in two distinct geotechnical centrifuge tests labeled inhere as Model A-20 g and Model B-45 g, conducted at 20 g and 45 g centrifuge levels, respectively. By employing the "modeling of models" approach, the primary aim of this paper is to investigate the effectiveness of centrifuge scaling laws, specifically the coupled dynamic and consolidation scaling laws, as well as the scaling laws for using viscous fluids in centrifuge testing of silty sand soils. This method evaluates the reliability of these scaling laws and tests the consistency of silty sand centrifuge experiments.

A secondary objective is to demonstrate that silty sand soil can be fully saturated using highly viscous fluids—a critical challenge for liquefaction studies. To address this, the paper introduces a bottom-up saturation technique utilizing geosynthetics attached to the sides of the model. The degree of saturation was assessed with a procedure developed by Okamura and Inoue [23], confirming the adapted procedure for saturating silty sand soils with viscous fluids.

These two tests are part of an extensive investigation into the effect of drainage on liquefaction behavior of sandy soils under field drainage conditions. Building on the foundational work by Ni et al. [24], Abdoun et al. [25], Ni et al. [26] on Ottawa F65 sand soil, this study extends the exploration to silty sand soils under possible field drainage conditions.

#### 2. Experimental program

Two centrifuge tests, Model A-20 g and Model B-45 g, were conducted to simulate the same prototype thickness of 5m at different gravitational levels, specifically at 20 g and 45 g respectively. This is a part of a project aimed at examining the impact of drainage on the liquefaction of silty sand soils under double drainage conditions. Both tests were under 1 atm overburden pressure, at the mid-depth of the soil layer. To achieve the desired overburden pressure, a layer of lead shot was placed over the silty sand layer being tested, as shown in Fig. 1. These experiments were designed to allow free drainage from both the top and bottom of the silty sand layer. The bottom drainage boundary was established by employing a Geocomposite layer (consisted of DuraFlow geonet coupled with a nonwoven needle-punched geotextile from Solmax (Houston, Texas)) and the Geonet strips, similar to the methodology described in Ni et al. [26].

Fig. 2 illustrates the setup including the geocomposite and the

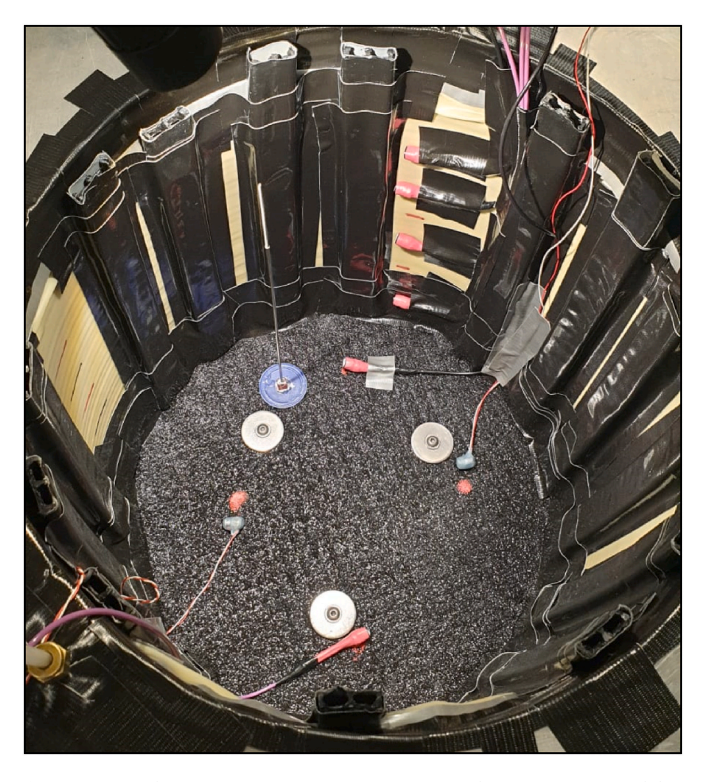


**Fig. 2.** Bottom drainage setup using Geocomposite and Geonet strips (Model A-20 g).

vertical geogrid strips arrangement prior to the pluviation of the silty sand, within the framework of a one-dimensional (1D) stacked ring laminar container at the geotechnical centrifuge facility of Rensselaer Polytechnic Institute (RPI).

Model A-20 g and Model B-45 g replicated this 5-m thickness under varying centrifuge g-levels of 20 and 45 g, respectively. All reported units for the centrifuge test are in prototype scale, aligning with the centrifuge scaling laws outlined by Tan and Scott [27], unless otherwise specified. The shaking input was applied at the base of the laminar container. Fig. 1 illustrates the experimental setup and configuration for both tests in model scale.

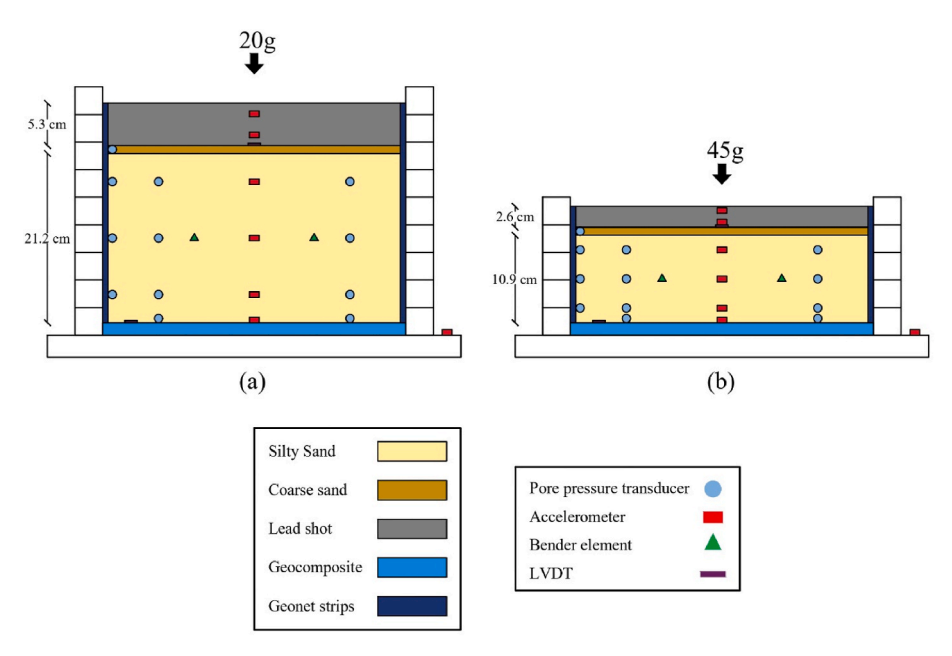


Fig. 1. Centrifuge Model Configuration in model scale; a) Model A-20 g; b) Test at Model B-45 g.

#### 2.1. Model layout

The two centrifuge experiments comprised three distinctive layers, as illustrated in Fig. 1: a lower layer of saturated and liquefiable silty sand, an intermediate thin layer of saturated transition coarse-sand, and an upper layer of dry lead shot. The preparation of the silty sand layer involved mixing of Ottawa F65 sand and Sil-Co-Sil 125 silt, as explained later herein. For both tests, the targeted relative density ( $D_r$ ) was 45 %, achieved at dry densities of 1640 kg/m³. Table 1 presents the precise relative density measurements obtained from both experiments. Density measurements were taken after reaching the targeted centrifuge acceleration g-level and before shaking the models. These measurements were conducted under the designated g-level and 1 atm effective stress ( $\sigma'_{vo}$ ) at the mid-depth of the silty sand layer.

Achieving the desired density involved a precisely calibrated dry pluviation process, adjusting the drop height and pluviation speed accordingly. After pluviation, the saturation of the silty sand layer was achieved using a viscous fluid, with appropriate viscosity based on the glevel, ensuring a 2–3 cm (measured in model scale) fluid accumulation above the silty sand to accommodate the subsequent transition layer. The transition coarse-sand layer was introduced directly into the viscous fluid, acting as a filter to prevent the infiltration of lead shot into the underlying silty sand. Any excess viscous fluid above the transition layer was carefully removed.

The top layer, consisting of approximately 1 m of dry lead shot, was then placed on top of the transition layer. The heavy lead shot (unit weight of  $62.6 \, \mathrm{kN/m^3}$ ) played a crucial role in attaining the necessary 1 atm at the mid-depth of the silty sand stratum before, during, and after shaking, all while preserving a free-drainage boundary throughout the entirety of the experiment.

#### 2.2. Silty sand

In this investigation, the silty sand utilized was prepared by mixing Ottawa F65 sand with Sil-Co-Sil 125 silt, both supplied by U.S. Silica, with the mix ratio set at 85 % sand and 15 % silt by weight. The specific gravity of this soil mix was measured in the laboratory facilities at Rensselaer Polytechnic Institute (RPI) and was found to be 2.64. Detailed grain-size analysis of the silty sand mixture was performed, revealing key parameters such as a  $D_{10}$  value of 0.035 mm and a  $D_{50}$  value of 0.192 mm. The maximum and minimum densities of the soil were found to be  $\rho_{max}=1985 \text{ kg/m}^3$  and  $\rho_{min}=1437 \text{ kg/m}^3$ , respectively. Permeability tests, conducted under 1 g conditions, yielded a permeability rate of  $6.4 \times 10^{-4} \text{ cm/s}$  at a relative density of 45 %.

## 2.3. Viscous fluid

The scaling principles for geotechnical centrifuge experiments stipulate the requirement of employing a viscous fluid to achieve saturation in both the silty sand and transition layers [5,27,28]. The viscosity of this fluid was tailored to the specific models, being 20 cp for Model A-20 g and 45 cp for Model B-45 g, to accurately simulate the prototype's permeability under field conditions at 1 g, following the guidelines set by Anderson [29].

The preparation of the viscous fluid involved mixing methylcellulose powder with water, creating a solution that mimicked the physical

$$\label{eq:Table 1} \begin{split} & \textbf{Table 1} \\ & D_r, \, PGA, \, V_s \, \text{and max. } r_u, \, \text{for both centrifuge tests.} \end{split}$$

Test	D <sub>r</sub> (%)	PGA at base (g)	Shear Wave Velocity (m/sec)	(r <sub>u</sub> ) <sub>max</sub>		
				Bottom	Middle	Top
Model A- 20 g	44.8	0.069	115	0.17	0.42	0.76
Model B- 45 g	42.3	0.064	116	0.19	0.41	0.67

properties of water, apart from its viscosity. The preparation of this mixture followed the procedure outlined by Adamidis and Madabhushi [30]. Subsequently, the viscosity of the prepared fluid was assessed using an automatic viscometer, which had been calibrated against two reference fluids of known viscosities.

## 2.4. Saturation technique

Achieving full saturation in the models proved to be particularly challenging, attributed to the silty sand's low permeability and the high viscosity of the saturation fluid. Ensuring models are fully saturated is essential, as the presence of air significantly influences liquefaction resistance [31]. To address these challenges, this study implemented a bottom-up saturation method. The saturation approach involved introducing the viscous fluid from the soil's base at a controlled rate, enabling the fluid to displace air while achieving saturation. The initial step involved sealing the laminar container, followed by the application of a robust vacuum pump to the model. Carbon dioxide was introduced into the evacuated model space to replace residual air. This sequence was repeated thrice, finished by the gradual injection of viscous fluid though one of the geonet strips affixed to the model's side, as shown in Fig. 3, ensuring thorough saturation under vacuum.

Given the complexities involved in determining the saturation level of the models, a method proposed by Okamura and Inoue [23] was adopted to assess the saturation level, particularly for the challenging scenario of using a 45 cp viscous fluid. This post-saturation evaluation technique employs a laser displacement sensor, specifically the Keyence LB-11 model with a resolution of  $10~\mu m$ . These measurements allow for an estimation of the remaining air volume within the model and, consequently, the degree of saturation. The air volume ( $V_1$ ) is calculated using Eq. (1):

$$V_1 = \frac{\Delta h}{(p_1/p_2) - 1} A$$
 Eq. 1

Where,  $V_1$  is the volume of air.

 $\Delta h$  is the change of the viscous fluid surface.

 $p_1, p_2$  are the container absolute pressures before and following the cessation of the vacuum process, respectively.

A is the area of the container.

The setup included a laser displacement sensor fixed to the sealing top of the container targeting a reflective surface for enhanced accuracy, which floats on the fluid surface. Measurements commenced prior to stopping the vacuum pump and continued as air was allowed back into the sealed container at a constant rate. The correlation between  $\Delta h$  and  $(p_1/p_2)-1$  is initially charted by Okamura and Inoue [23], and shown in Fig. 4. Three curves are originally presented: one for a test involving only water and the other two for Keisha no.8 soil (fine sand with fines contents 13.5 %) models saturated under different vacuum pressures. The soil was compacted to a relative density of 60 % for these two



Fig. 3. Saturation tube through the geonet strips.

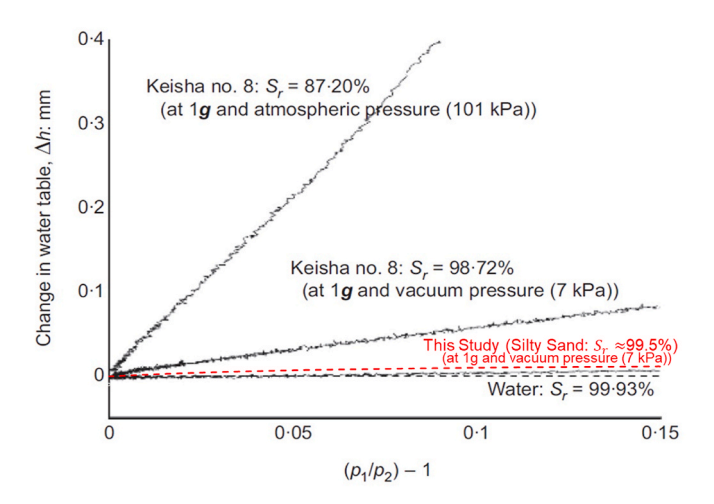


Fig. 4. Relationship between change in viscous fluid surface and pressure in the container (modified after [23]).

experiments. The water-only test achieved a near-complete saturation of 99.93 %, whereas the Keisha no.8 soil model, saturated at atmospheric pressure, reached 87.2 % saturation, and the model subjected to a vacuum pressure of 7 kPa achieved 98.72 % saturation. In the cited graph, the slope of the lines correlates directly with the volume of air. The result from this study is overlaid in a red dotted line. Fig. 4 indicates that the saturation level of silty sand from this study not only surpassed that of the Keisha no.8 soil models but also closely matched the trend and saturation percentages of the water-only test. The estimated saturation degree  $(S_r)$  for the silty sand, achieved through the use of viscous fluid, was nearly 99.5 %. The close correlation between this study's saturation and the water-only model indicates the exceptional efficacy of the bottom-up saturation technique employed in this research. The enhanced saturation results obtained in this investigation may be attributed to the introduction of carbon dioxide before the start of the saturation, applied three times before commencing the saturation process. This preparatory step, which was not utilized in the Keisha no.8 soil experiments, may have significantly contributed to the higher degree of saturation achieved.

Moreover, this degree of saturation, examined at 1 g, showcases the potential for even greater saturation levels once the lead shot layer is added and the model is subjected to the centrifugal forces within the geotechnical centrifuge. This finding underlines the success of saturation technique utilized herein, highlighting its effectiveness in saturating low permeable soil using viscous fluid.

## 2.5. Instrumentation

The centrifuge experiments conducted in this research were designed with detailed instrumentation to enable extensive data collection and analysis. Each model was prepared with a comprehensive set of transducers, including accelerometers, Pore Pressure Transducers (PPTs), Linear Variable Differential Transformers (LVDTs) for measuring vertical displacement, and bender elements for measuring the shear wave velocity. The arrangement of these instruments is illustrated in Fig. 1.

Acceleration responses were captured using sixteen accelerometers distributed across the model. Four of these were located at the container's base to record the shaker's input motion in three dimensions, with specific alignment to the direction of shaking. The soil itself housed eight accelerometers, arranged in two vertical arrays of four sensors each, to track acceleration at various depths within the silty sand layer, covering the base, bottom, middle, and top sections. Additionally, four accelerometers were installed within the lead shot layer to monitor its response and assist in subsequent calculations of shear stresses and strains.

Pore pressure changes within the saturated silty sand were monitored by twelve PPTs, arranged in three vertical arrays. One of these arrays was fixed to the laminar container's inner wall, and the other two were positioned symmetrically around the silty sand layer. This setup, with three PPTs near both the top and bottom of the silty sand layer, was designed to comprehensively map pressure variations throughout the depth of the layer.

Settlements due to changes in effective stress during the centrifuge's spinning-up, and shaking phases were measured using two LVDTs located on the transition layer. An additional LVDT was placed at the base of the silty sand layer to observe any settlement in the Geocomposite layer.

#### 2.6. Shaking events

In both experiments, a one-dimensional (1D) shaking was initiated from the base using the centrifuge's in-flight shaker system. The input motion for these shaking events was uniform sinusoidal waves, consisting of 10 cycles with a dominant prototype frequency of 2 Hz. The Peak Ground Acceleration (PGA) for both tests are reported in Table 1.

#### 2.7. Shear-wave velocity

Shear wave velocity  $(V_s)$  measurements within the silty sand layer were performed by bender elements placed at the mid-depth, where the effective overburden pressure reaches 1 atm. This system utilized a pair of transducers: one to emit shear waves and another to receive them, allowing for accurate determination of the soil's shear wave velocity prior to shaking. The calculated velocities are presented in Table 1. In both models, the shear wave velocity was evaluated using the "first arrival" method [32,33]. The estimation of horizontally propagating vertically polarized  $V_s$  was derived from the time taken for wave propagation and the distance between the transmitting and receiving elements. In Model A-20 g and Model B-45 g,  $V_s$  was estimated to be 115 m/s and 116 m/s, respectively, underscoring the homogeneity of the soil properties across the different centrifuge experiments.

#### 3. Results

This section examines the key findings and initial analyses from both centrifuge experiments, exploring various aspects including acceleration, excess pore pressure, volumetric strain in the vertical direction, shear stress ratio, and shear strains. It provides an in-depth analysis of the data collected, and observations made, highlighting the equivalence in outcomes from both tests.

#### 3.1. Acceleration

Fig. 5 displays the acceleration time histories for both Model A-20 g and Model B-45 g experiments, illustrating the acceleration histories at various depths of the silty sand layer, including the base, bottom, middle, and top, scaled to the prototype. Acceleration data was collected using accelerometers embedded at these different levels within the layer.

The plot shows that the input is a sinusoidal waveform consisting of 10 cycles over a 5-s duration, indicative of a 2 Hz frequency. Fig. 5 shows consistency in the waveform across both models underscores the uniformity and reproducibility of the input motion at the base. Wave propagation from the base upwards through the layer shows excellent similarities in both models. According to Table 1, the Peak Ground Acceleration (PGA) at the base for both the Model A-20 g and Model B-45 g closely matches, with values of 0.069 g and 0.064 g, respectively.

Analysis of the acceleration time histories within the silty sand, as shown in Fig. 5, reveals a slight amplification in peak acceleration moving from the base to the top especially at the beginning of the shake. After 1-2 s into the shaking, the acceleration starts to attenuate, as the

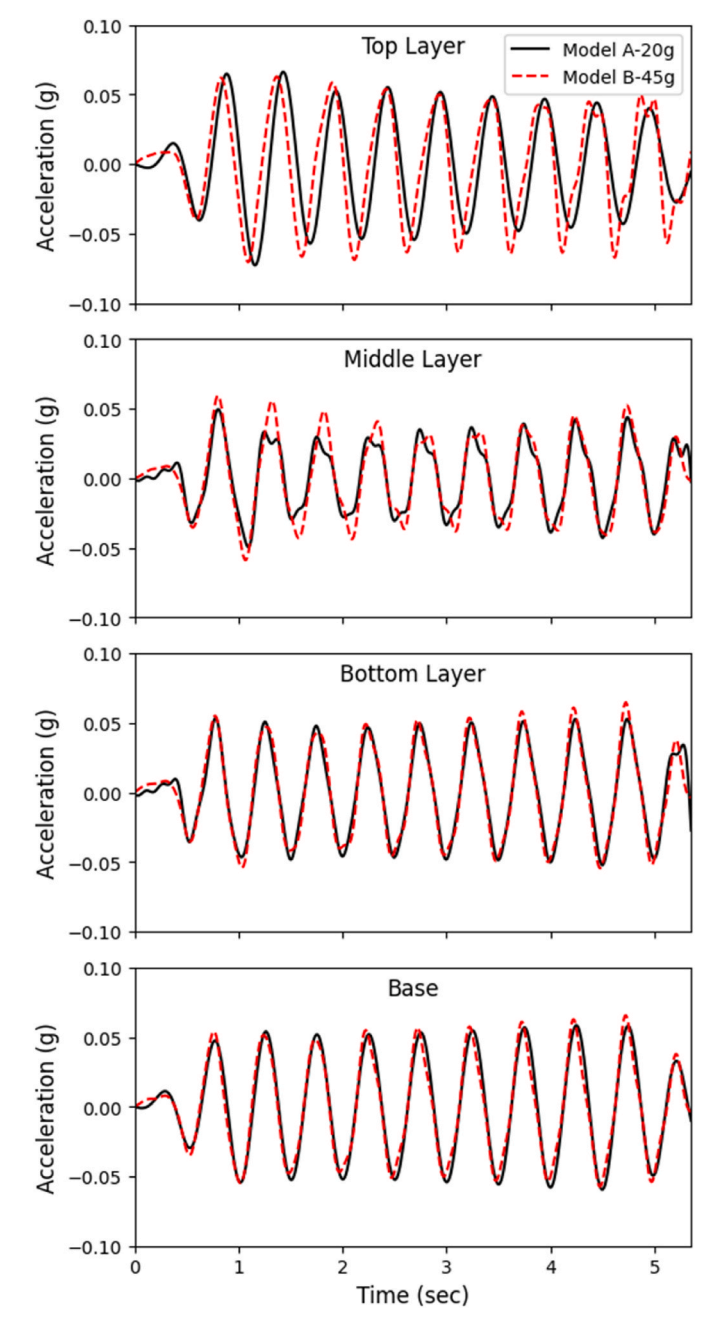


Fig. 5. Comparison between acceleration time histories at various depths for both tests.

excess pore pressure starts to increase.

#### 3.2. Excess pore water pressure time histories

Fig. 6 showcases the development of the excess pore pressure ratio  $(r_u)$  over the course of the shaking events and during the dissipation period for both Model A-20 g and Model B-45 g experiments. The displayed  $r_u$  values correspond to the locations of the pore pressure transducers, which are targeted to be the same elevations as the accelerometers detailed in Fig. 5. The excess pore pressure ratio is determined by dividing the observed excess pore pressure (u) by the initial pre-shaking effective overburden pressure  $(\sigma_v')$  at each sensor's depth.

Fig. 6-a captures the first 6 s, showing the buildup in excess pore pressure during the shaking. The data indicates similar patterns across

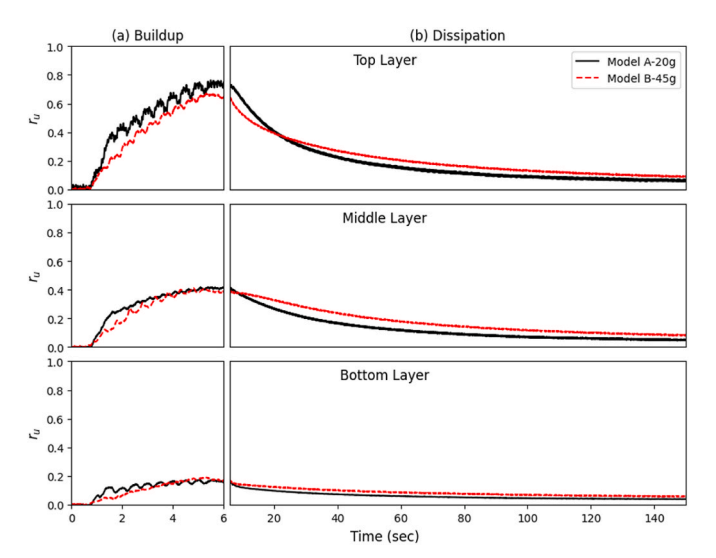


**Fig. 6.** Excess pore pressure ratio time histories a) buildup phase, b) dissipation phase.

both models, with  $r_u$  values being notably higher at the soil's top, decreasing towards the middle, and lowest at the bottom. Table 1 displays the maximum excess pore pressure ratio  $(r_u)_{max}$  at various depths—bottom, middle, and top—illustrating a uniform liquefaction behavior in both tests at the bottom and middle depths. Minor variations observed at the top are attributed to the placement of sensors, a detail that will be further explored in the following section.

Fig. 6-b presents the  $r_u$  values immediately following the end of shaking, illustrating the dissipation of the excess pore pressure ratio. This portion underscores the significant parallel trend of excess pore pressure dissipation across both models, reinforcing the robustness and consistency of the dissipation fluid flow.

Despite variations in model thickness (in model scale) and the viscosity of the fluids used in each experiment, the resemblance observed in both tests—particularly during the phases of excess pore pressure buildup and dissipation—indicates that the models achieved a comparable level of saturation, which can be inferred as full saturation. This observation underscores the success of the adopted saturation techniques introduced in this study, demonstrating their capability to achieve consistent results across models of different thicknesses.

## 3.3. Excess pore water pressure profiles

Fig. 7-a and Fig. 7-b present isochrone charts that map the excess pore pressure (u) against depth (z) at selected time intervals during the seismic events, with both u and z values uniformly scaled and depth adjusted relative to the soil layer thickness for straightforward comparison across tests. These charts include the Effective stress line (marking the onset of initial liquefaction) at an  $r_u$  value of 1.0, as well as the total stress line. The normalized depth scale starts at 0 for the silty sand layer's surface and extends to 1 at the soil layer's base. Excess pore pressure at the layer's top was plotted through linear interpolation between the uppermost PPT readings and the PPT sensor located in the transition layer. The selected time steps (1.5, 2.5, and 5 s) illustrate that the top of the silty sand layer is consistently closer to reaching liquefaction conditions, followed by the middle section, with the bottom displaying the lowest susceptibility. Fig. 7 notably demonstrates the very good consistency in excess pore pressure values and trends between the two experiments.

Fig. 8-a and Fig. 8-b display the dissipation isochrones of excess pore water pressure post-shaking, spanning from 0 to 480 s, with time ( $t_{\rm diss}$ ) zero marking the cessation of the shake. These isochrones, similar to the buildup plots in Fig. 7, utilize depth normalization and include lines for

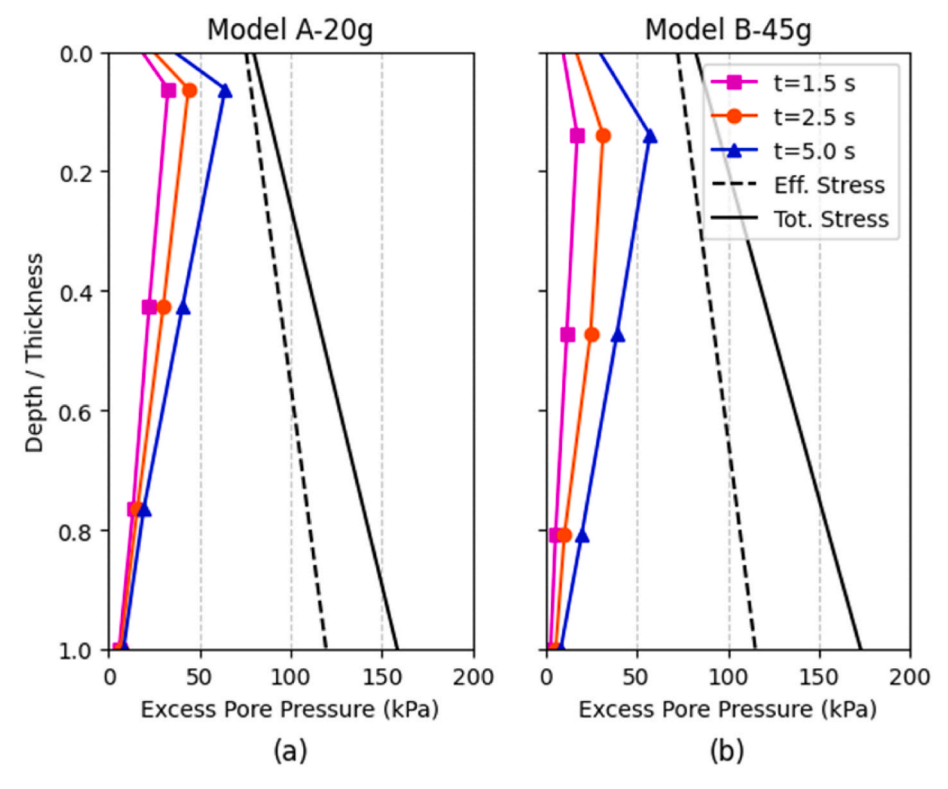


Fig. 7. Excess pore pressure profiles (isochrones) during buildup, a) Model A-20 g; b) Model B-45 g.

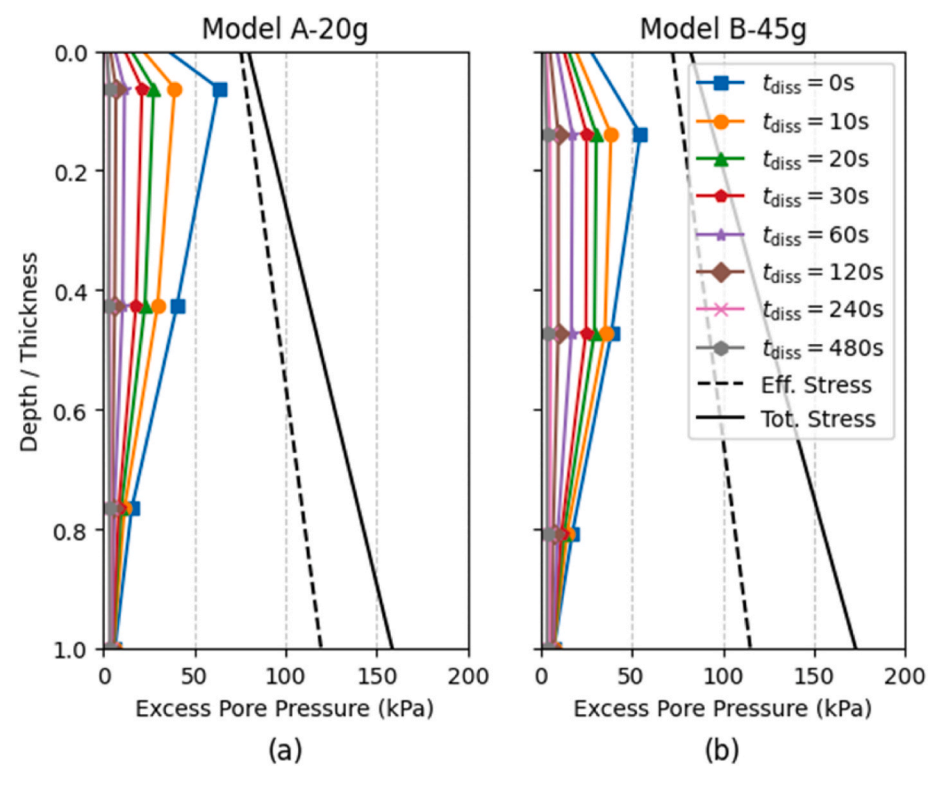


Fig. 8. Excess pore pressure profiles (isochrones) during dissipation, a) Model A-20 g; b) Model B-45 g.

effective and total stress. The very good similarities in dissipation patterns across both tests are apparent. Excess pore pressure readings at the silty sand layer's boundaries, as shown in Figs. 7 and 8, consistently indicate minimal pressure, confirming the effectiveness of the free-drainage conditions established for the experiments.

Fig. 9-a and Fig. 9-b illustrate the profiles of maximum excess pore pressure and the associated  $r_u$  values at varying depths, with each depth normalized by the thickness of the soil layer in the respective models. Although Table 1 indicates minor discrepancies in the maximum pore pressure ratio  $(r_u)_{max}$  at the top layer of the silty sand, Fig. 9-a and 9-b,

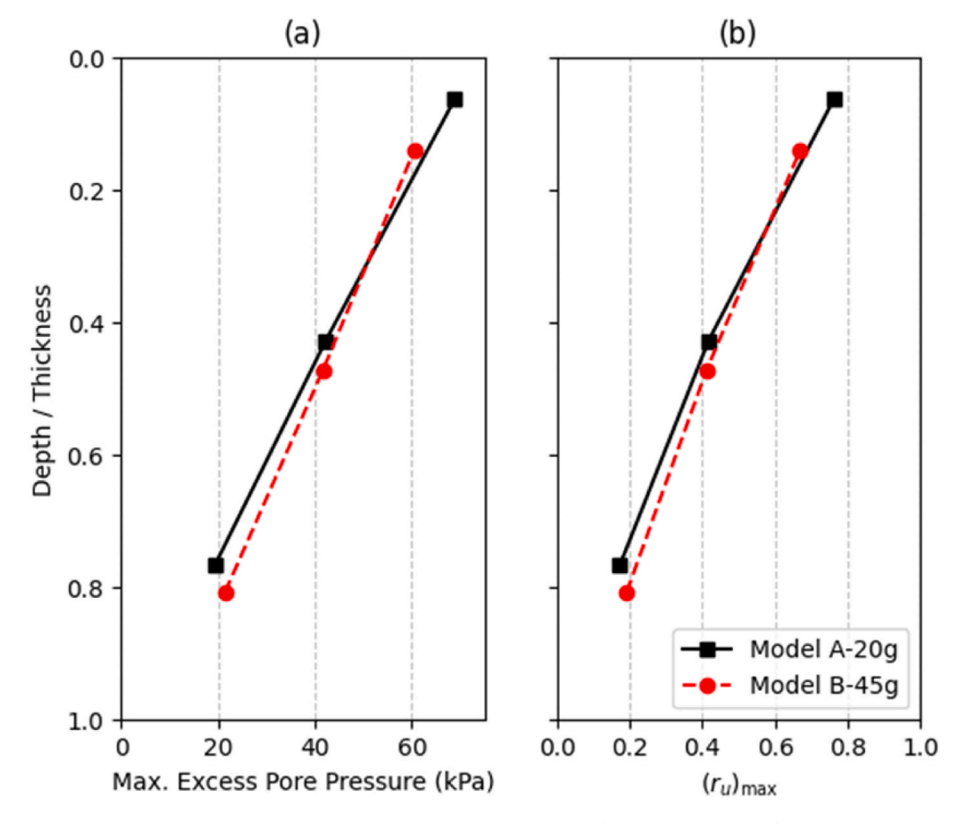


Fig. 9. (a) Max. Excess Pore Water Pressure profile; (b) max.  $R_{\rm u}$  profile.

which are normalized by the depth of each test, exhibit significant alignment in both excess pore pressure and maximum excess pore pressure ratio. This observation clarifies that the variations documented in Table 1 arise from differences in sensor depth placement. When these measurements are graphically represented as profiles, it becomes evident that the data points align, adhering to the same trend and

matching in value, thus underscoring the uniformity of the soil's response in both models.

## 3.4. Volumetric strain

Settlement measurements within the silty sand layer were captured

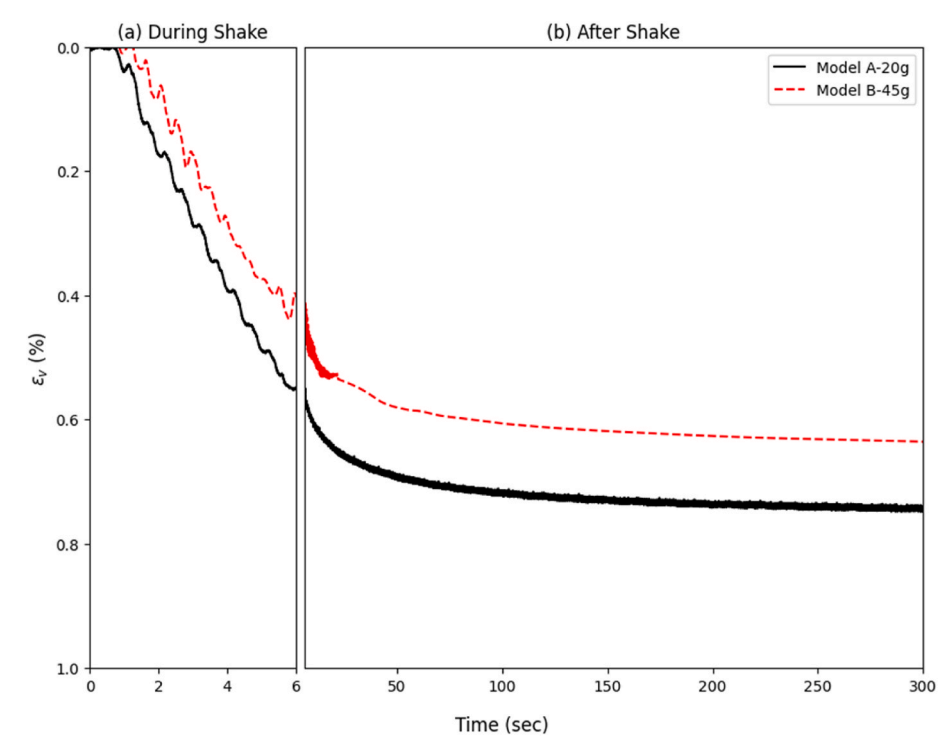


Fig. 10. Vertical Normal Strain, a) during shake; b) after shake.

using LVDTs placed atop the transition layer. The decision against placing LVDTs directly on the silty sand layer's surface was due to the risk of the devices sinking into the loose silty sand during seismic events, which could compromise the accuracy of the data. To precisely determine the alteration in soil thickness, readings from the base LVDT—nearly negligible and close to zero—were subtracted from the top LVDT measurements. This process was undertaken to factor in any settlement occurring in the Geocomposite layer located underneath the silty sand layer.

Fig. 10 illustrates the normalized settlement, depicted as volumetric strain in the vertical direction over time, commencing with the start of the seismic activity. The volumetric strain in the vertical direction was derived by dividing the LVDT-recorded settlement by the silty sand layer's thickness in each model. Fig. 10 illustrates the settlement patterns, highlighting that the initiation of settlement in Model A-20 g preceded that of Model B-45 g. This discrepancy can be linked to the earlier onset of acceleration waves in Model A-20 g, as depicted by the base acceleration data in Fig. 5. Additionally, Model A-20 g exhibited marginally higher settlement levels compared to Model B-45 g, potentially attributed to a slightly higher PGA value for Model A-20 g, as indicated in Table 1. Nonetheless, the settlement pattern remains consistent across both models, with settlement ceasing around 300 s after shaking onset.

#### 3.5. Stress ratio & shear strain

In this study, the shear stresses and strains for both centrifuge tests were determined using the acceleration time histories recorded by sensors embedded within the silty sand and the lead shot layer. This data was processed through the system identification (SI) technique, a method pioneered by Elgamal et al. [34], Zeghal et al. [35], Elgamal et al. [36], which conceptualizes the level deposit under dynamic loading as a shear beam. Subsequently, the shear stress ratio was computed by dividing the obtained shear stress by the initial effective vertical stress. The time histories of the shear stress ratios at varying depths of the silty sand layer are illustrated in Fig. 11, while the corresponding shear strain time histories are presented in Fig. 12.

The median undegraded Cyclic Stress Ratio (CSR) for both tests, at different depths, is tabulated in Table 2. Notably, an observable degradation in stress was identified in the initial shaking cycles for Model A-20 g, as depicted in Fig. 11. While the degradation in stress was less pronounced in Model B-45 g, CSR calculations for this model also focused on the initial cycles for comparison with Model A-20 g. Consequently, the undegraded CSR values were used for calculating the median values presented in Table 2. This approach aligns with the methodology outlined by Ni et al. [24], Ni [37], emphasizing the importance of a total stress analysis that abandons the stress-strain degradation due to pore pressure buildup.

The stress analysis, which neglects the shear stress degradation due to excess pore pressure is the most used analysis technique in practice due to its simplicity. By focusing on the initial loading cycles in the centrifuge experiments herein, the analysis avoids the complications introduced by shear stress degradation after the first few cycles when the excess pore pressure increases significantly [24]. This allows for a more representative and consistent estimation of the cyclic shear stress ratio of the soil in centrifuge experimental simulation.

The shear strain graphs presented in Fig. 12 display a notable alignment between the two tests, with the exception of the first two cycles where Model A-20 g consistently exhibits higher lower values compared to Model B-45 g. This is consistent with the slightly higher acceleration, excess pore pressure and settlement observed for Model A-20 g.

#### 4. Discussion

This paper presents two centrifuge experiments, specifically

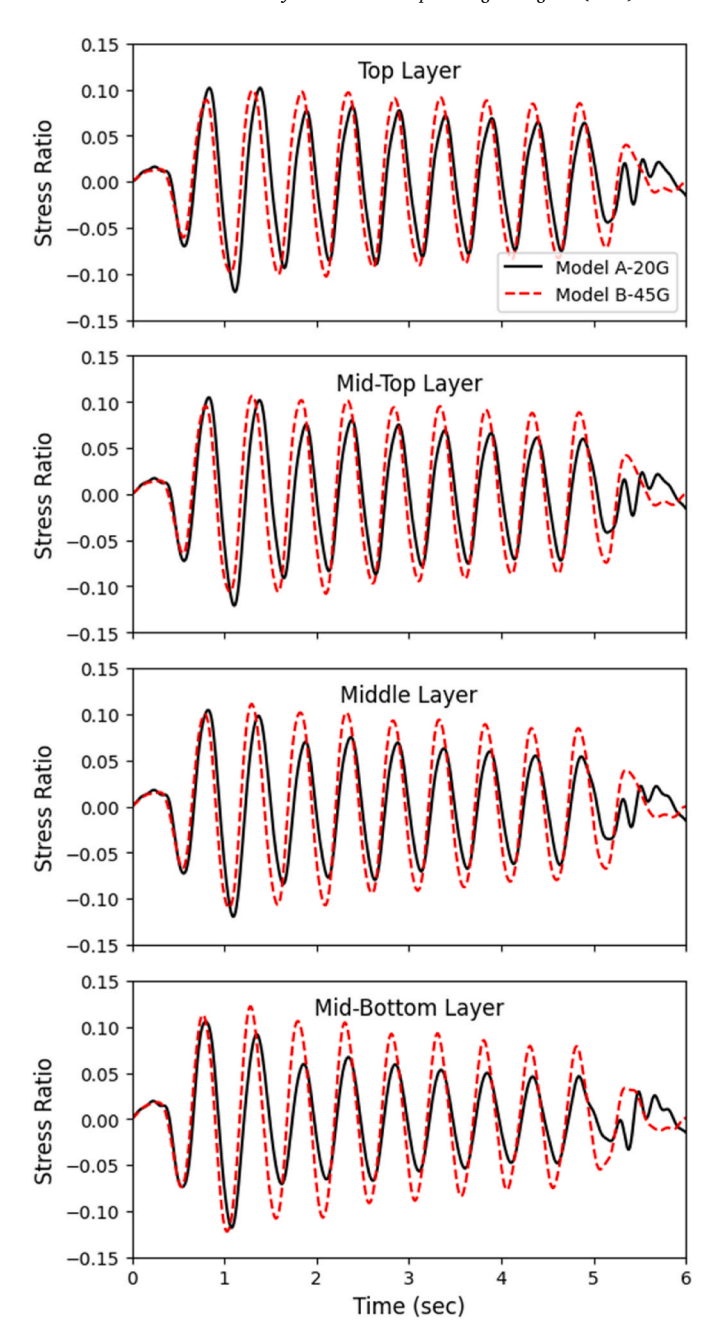
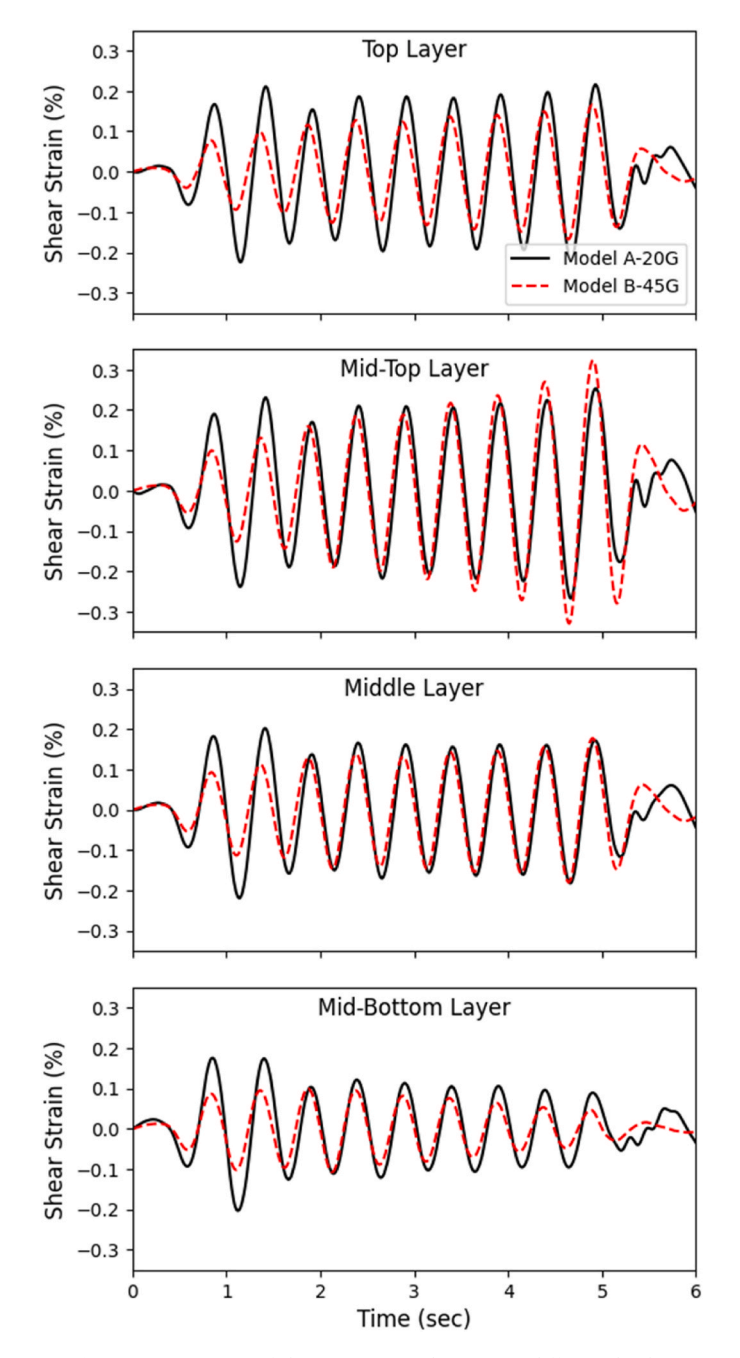


Fig. 11. Comparison of shear stress ratio time histories at different depths.

designed to explore the behavior of silty sand under seismic loading conditions. Each of the experiments were subjected to different centrifugal accelerations (20 g and 45 g) and were involved in investigating the dynamic response and fluid flow within the silty sand soil under double drainage conditions. The core of the analysis focuses on the measurement of excess pore pressure and its dissipation over time, a critical indicator of soil's susceptibility to liquefaction and subsequent consolidation behavior.

By applying scaling laws that account for the dynamic behavior and fluid flow in the models, the study ensured that the observed phenomena could be accurately scaled to the same prototype conditions. The use of instrumentation arrays, including Pore Pressure Transducers (PPTs) placed within the soil, provided precise data on the buildup and dissipation of excess pore pressure due to seismic shaking. This data, when analyzed, revealed a remarkable consistency in the behavior of excess pore pressure dissipation between the two models, despite the differences in centrifugal forces applied.



 $\textbf{Fig. 12.} \ \ \textbf{Comparison of shear strain time histories at different depths}.$ 

Table 2 CSR Data for both tests.

Test	Median CSR					
	Mid-Bottom	Middle	Mid-Top	Top		
Model A-20 g Model B-45 g	0.092 0.113	0.098 0.107	0.102 0.106	0.102 0.100		

The scaling laws for viscous fluids were crucial in this context. These laws ensure that the fluid flow within the models accurately represents the flow that would occur in field conditions, taking into account the viscosity of the pore fluid and the scale of the model. The close correlation in excess pore pressure buildup and dissipation observed between the two centrifuge tests provides a robust validation of the coupled dynamic and consolidation scaling laws, as well as the scaling laws for

viscous fluids. This outcome highlights the precision and reliability of the centrifuge modeling techniques employed as well as the repeatability of tests within this project.

The saturation of both models was achieved using a bottom-up technique, demonstrating its efficacy in saturating silty sand soil with a viscous fluid through a method proposed by Okamura and Inoue [23]. This method provides a reliable estimate of the saturation degree. Moreover, the consistency in the buildup observed across the two tests indicates that both models, despite their differing thicknesses at the model scale (but not at the prototype scale), attained equivalent degrees of saturation. This observation underscores the effectiveness of the employed saturation technique.

The analysis of shear stress and strain in both experiments was carried out using the system identification method, employing an array of accelerometers embedded within the silty sand and lead shot layers. By computing the stress ratio and shear strain across various depths of the silty sand layer, data was plotted to illustrate the behavior under seismic loading. Furthermore, the median values of the undegraded cyclic stress ratios (CSR) for both tests were determined, showcasing the effectiveness of the system identification technique in capturing the soil's response at differing centrifuge acceleration levels.

#### 5. Summary and conclusions

Two models, Model A-20 g and Model B-45 g, of saturated silty sand, were tested in the centrifuge facility of Rensselaer Polytechnic Institute (RPI) to study the liquefaction behavior of silty sand under a double drainage condition. Both experiments, designed to replicate the same prototype at different g-levels, employing the "modeling of models" technique. Both models aimed to assess the silty sand soil's behavior under 1 atm overburden pressure at the soil's mid-height, under double drainage conditions. The methodology for both experiments was uniformly applied, ensuring comparability. The main outcomes of this investigation reveal.

- The measured shear wave velocity data and the measured mass density from both tests closely align, highlighting the reproducibility of the relative density achieved in each model and emphasizing the experiments' consistency.
- Bottom-up saturation technique was employed to ensure complete saturation of the silty sand models with viscous fluid, a crucial step for the analysis of liquefaction. For the most challenging scenario—achieving saturation using a 45 cp viscous fluid—the saturation level was determined by means of a methodology developed by Ni et al. [26]
- The saturation achieved in this study was benchmarked against three
  different tests from the previously cited research, it was observed
  that the degree of saturation closely mirrored that of the model using
  only water and exceeded the saturation levels of the other two sand
  models reported by Okamura and Inoue [23]. This analysis
  confirmed the effectiveness of the bottom-up method in attaining
  higher saturation levels.
- Remarkable consistency was observed across both centrifuge models, in the silty sand layer's response, including acceleration profiles, the buildup and dissipation of excess pore pressure, and the analysis of shear stress ratios and strains.
- The consistency observed in both tests, particularly throughout the
  excess pore pressure buildup and dissipation stages, suggests a uniform saturation level across both models. This highlights the efficiency of the saturation methods presented in this study, further
  validating their effectiveness.
- The coupled dynamic and consolidation scaling laws, alongside the scaling laws for viscous fluids, were confirmed by the close correlation in excess pore pressure dissipation post-shaking between the two tests.

#### CRediT authorship contribution statement

Mohamed E. Ghazy: Writing – original draft, Visualization, Validation, Methodology, Investigation, Formal analysis, Data curation, Conceptualization. Tarek Abdoun: Writing – review & editing, Visualization, Supervision, Resources, Project administration, Funding acquisition, Conceptualization. Ricardo Dobry: Writing – review & editing, Visualization, Project administration, Investigation, Funding acquisition, Conceptualization. Waleed El-Sekelly: Writing – review & editing, Writing – original draft, Visualization, Supervision, Project administration, Methodology, Investigation, Conceptualization.

### Declaration of competing interest

The authors declare that they have no known competing financial interests or personal relationships that could have appeared to influence the work reported in this paper.

## Data availability

Data will be made available on request.

## Acknowledgments

The authors wish to express their gratitude to the RPI geotechnical centrifuge technical staff, especially Mr. Kyle Weichold, for their invaluable assistance with physical centrifuge modeling, as well as their support throughout the project. The authors also would extend their gratitude to Dr. Heba Ali's assistance in clarifying the nuances of centrifuge modeling and its technical aspects is greatly valued. Additionally, the authors would like to thank Solmax.com for providing all geocomposite and geonet materials used in the research project, which is greatly appreciated. The research was supported by the National Science Foundation under Grant No. 1545026 and 1904313. This work was partially supported by the Sand Hazards and opportunities for Resilience, Energy, and Sustainability (SHORES) Center, funded by Tamkeen under the NYUAD Research Institute Award CG013.

## References

- [1] Schofield AN. Dynamic and earthquake geotechnical centrifuge modelling. In:
  Presented at the international conference on recent advances in geotechnical
  earthquake engineering and soil dynamics, Missouri; 1981 [Online]. Available: htt
  ps://scholarsmine.mst.edu/icrageesd/01icrageesd/session05/2.
- [2] Schofield AN. Cambridge geotechnical centrifuge operations. Geotechnique 1980; 30(3):227–68. https://doi.org/10.1680/geot.1980.30.3.227.
- [3] Kutter BL. Recent advances in centrifuge modeling of seismic shaking. In: Presented at the international conferences on recent advances in geotechnical earthquake engineering and soil dynamics, Missouri; 1995 [Online]. Available: htt ps://scholarsmine.mst.edu/icrageesd/03icrageesd/session16/4.
- [4] Hon-Yim K. Summary of the state-of-the-art in centrifuge model testing. In: Centrifuges in soil mechanics. CRC Press; 2020. p. 11–8.
- [5] Taylor RN. Centrifuges in modelling: principles and scale effects. In: Geotechnical centrifuge technology. London: CRC Press; 1994. p. 19–33.
- [6] Madabhushi GSP. Centrifuge modelling for civil engineers. first ed. London: CRC Press; 2015. p. 324.
- [7] Barton YO. Response of pile groups to lateral loading in the centrifuge. 1985.
- [8] Nunez IL, Phillips R, Randolph MF, Wesselink BD. Modelling laterally loaded piles in calcareous sand. CUED/D-Soils: Cambridge University, Engineering Department; 1987.
- [9] Terashi M, Kawabata K, Kitazume M. Centrifuge modeling of a laterally loaded pile. In: Presented at the 12th international conference on soil mechanics and foundation engineering; 1989. Rio De Janeiro.
- [10] Ketcham SA, Black PB, Pretto R. Frost heave loading of constrained footing by centrifuge modeling. J Geotech Geoenviron Eng 1997;123(9):874–80. https://doi org/10.1061/(ASCE)1090-0241(1997)123:9(874).
- [11] Yang D, Goodings DJ. Climatic soil freezing modeled in centrifuge. J Geotech Geoenviron Eng 1998;124(12):1186–94. https://doi.org/10.1061/(ASCE)1090-0241(1998)124:12(1186).

- [12] Krishnaiah S, Singh DN. Centrifuge modelling of heat migration in soils. Int J Phys Model Geotech 2004;4(3):39–47. https://doi.org/10.1680/ijpmg.2004.040303.
- [13] Dayarathne R, Hawlader B, Phillips R. Centrifuge modelling of gas pipelines undergoing freeze-thaw cycles. Can Geotech J 2022;59(4):485–97. https://doi. org/10.1139/cgj-2020-0482.
- [14] Bowman ET, Laue J, Imre B, Springman SM. Experimental modelling of debris flow behaviour using a geotechnical centrifuge. Can Geotech J 2010;47(7):742–62. https://doi.org/10.1139/t09-141.
- [15] Zhang W, Askarinejad A. Centrifuge modelling of static liquefaction in submarine slopes: scaling law dilemma. Can Geotech J 2021;58(2):200–9. https://doi.org/ 10.1139/cgi-2019-0417.
- [16] Ovalle-Villamil W, Sasanakul I. Assessment of centrifuge modelling of internal erosion induced by upward flow conditions. Int J Phys Model Geotech 2021;21(5): 251–67. https://doi.org/10.1680/jphmg.20.00004.
- [17] Alisawi AT, Collins PEF, Cashell KA. Novel methodology for scaling and simulating structural behaviour for soil-structure systems subjected to extreme loading conditions. Appl Sci 2023;13(15):8626 [Online]. Available: https://www.mdpi. com/2076-3417/13/15/8626.
- [18] Iai S, Tobita T, Nakahara T. Generalised scaling relations for dynamic centrifuge tests. Geotechnique 2005;55(5):355–62. https://doi.org/10.1680/ geot.2005.55.5.355.
- [19] Tobita T, Iai S, Nishida K. Verification of generalized scaling relations for dynamic centrifuge experiments. 2007.
- [20] Korre E, Abdoun T, Zeghal M, Kokkali P. Verification of generalized scaling laws: two centrifuge tests of a liquefiable sloping deposit. Soil Dynam Earthq Eng 2021; 141:106480. https://doi.org/10.1016/j.soildyn.2020.106480.
- [21] Tobita T, et al. LEAP-ASIA-2019: validation of centrifuge experiments and the generalized scaling law on liquefaction-induced lateral spreading. Soil Dynam Earthq Eng 2022;157:107237. https://doi.org/10.1016/j.soildyn.2022.107237.
- [22] Ma Q, Zhou Y-G, Yang X-T, Chen Y-M. A state parameter-based scaling law for centrifuge modelling. Soil Dynam Earthq Eng 2022/11/01/2022;162:107487. https://doi.org/10.1016/j.soildyn.2022.107487.
- [23] Okamura M, Inoue T. Preparation of fully saturated models for liquefaction study. Int J Phys Model Geotech 2012;12(1):39–46. https://doi.org/10.1680/ ijpmg.2012.12.1.39.
- [24] Ñi M, Abdoun T, Dobry R, Zehtab K, Marr A, El-Sekelly W. Pore pressure and ko evaluation at high overburden pressure under field drainage conditions. I: centrifuge experiments. J Geotech Geoenviron Eng 2020;146(9):04020088. https://doi.org/10.1061/(asce)gt.1943-5606.0002303.
- [25] Abdoun T, Ni M, Dobry R, Zehtab K, Marr A, El-Sekelly W. Pore pressure and kon evaluation at high overburden pressure under field drainage conditions. II: additional interpretation. J Geotech Geoenviron Eng 2020;146(9):04020089. https://doi.org/10.1061/(asce)gt.1943-5606.0002302.
- [26] Ni M, Abdoun T, Dobry R, El-Sekelly W. Effect of field drainage on seismic pore pressure buildup and kσ under high overburden pressure. J Geotech Geoenviron Eng 2021;147(9):04021088. https://doi.org/10.1061/(asce)gt.1943-5606.0002536.
- [27] Tan TS, Scott RF. Centrifuge scaling considerations for fluid-particle systems. Geotechnique 1985;35(4):461–70. https://doi.org/10.1680/geot.1985.35.4.461.
- [28] Kutter BL. Dynamic centrifuge modeling of geotechnical structures. Transport Res Rec 1992;1336.
- [29] Anderson J. Fundamentals of aerodynamics (SI units). McGraw hill; 2011.
- [30] Adamidis O, Madabhushi GSP. Use of viscous pore fluids in dynamic centrifuge modelling. Int J Phys Model Geotech 2015;15(3):141–9. https://doi.org/10.1680/ iphme.14.00022
- [31] Yoshimi Y, Tanaka K, Tokimatsu K. Liquefaction resistance of A partially saturated sand. Soils Found 1989/09/01/1989;29(3):157–62. https://doi.org/10.3208/ sandf1972 29 3 157
- [32] El-Sekelly W, Abdoun T, Dobry R. Soil characterization in centrifuge models through measurement of shear wave velocities using bender elements. In: GeoCongress 2012; 2012. p. 2037–47. https://doi.org/10.1061/ 9780784412121.209. https://ascelibrary.org/doi/abs/10.1061/97807844 12121.209.
- [33] El-Sekelly W, Tessari A, Abdoun T. Shear wave velocity measurement in the centrifuge using bender elements. Geotech Test J 2014;37(4):20130189. https:// doi.org/10.1520/gtj20130189.
- [34] Elgamal A-W, Zeghal M, Tang HT, Stepp JC. Lotung downhole array. I: evaluation of site dynamic properties. Journal of Geotechnical Engineering 1995;121(4): 350–62. https://doi.org/10.1061/(ASCE)0733-9410(1995)121:4(350).
- [35] Zeghal M, Elgamal A-W, Tang HT, Stepp JC. Lotung downhole array. II: evaluation of soil nonlinear properties. Journal of Geotechnical Engineering 1995;121(4): 363–78. https://doi.org/10.1061/(ASCE)0733-9410(1995)121:4(363).
- [36] Elgamal A, Zeghal M, Taboada V, Dobry R. Analysis of site liquefaction and lateral spreading using centrifuge testing records. Soils Found 1996/06/01/1996;36(2): 111–21. https://doi.org/10.3208/sandf.36.2\_111.
- [37] Ni M. Centrifuge modeling of seismic liquefaction of clean Ottawa sand under low and high confining pressures for field conditions. United States – New York: Ph.D., Rensselaer Polytechnic Institute; 2020, 27995324 [Online]. Available:.